Laser and Particle Beams (2003), *21*, 437–442. Printed in the USA.

DOI: 10.1017/S0263034603213239

Numerical methods for the determination of mixing

E. GEORGE,[1] J. GLIMM,[1] X.L. LI,[1] A. MARCHESE,[1] Z.-L. XU,[1] J.W. GROVE,[2] AND DAVID H. SHARP[3]

[1]Department of Applied Mathematics and Statistics, Stony Brook University, Stony Brook, New York
[2]Computer and Computational Science Division, Los Alamos National Laboratory, Los Alamos, New Mexico
[3]Theoretical Division, Los Alamos National Laboratory, Los Alamos, New Mexico

(RECEIVED 28 March 2002; ACCEPTED 4 April 2003)

Abstract

We present a Rayleigh–Taylor mixing rate simulation with an acceleration rate falling within the range of experiments. The simulation uses front tracking to prevent interfacial mass diffusion. We present evidence to support the assertion that the lower acceleration rate found in untracked simulations is caused, at least to a large extent, by a reduced buoyancy force due to numerical interfacial mass diffusion. Quantitative evidence includes results from a time-dependent Atwood number analysis of the diffusive simulation, which yields a renormalized mixing rate coefficient for the diffusive simulation in agreement with experiment. We also present the study of Richtmyer–Meshkov mixing in cylindrical geometry using the front tracking method and compare it with the experimental results.

Keywords: Front tracking; Numerical diffusion; Rayleigh–Taylor instability; Richtmyer–Meshkov instability

1. INTRODUCTION

Since Read (1984) and Youngs (1984) published the first experimental study of Rayleigh–Taylor instability with a randomly perturbed fluid interface, attention has been drawn to the nondimensional acceleration rate of the bubble envelope. Assume that two fluids are separated by a randomly perturbed interface and that the gravitational field points from the heavy fluid ρ_H to the light fluid ρ_L. Read and Youngs confirmed the Sharp–Wheeler theoretical prediction (1961, unpublished technical report, Institute of Defense Analyses) that the average bubble front moves with acceleration scaling

$$h(t) = \alpha A g t^2, \tag{1}$$

where h is the height of the bubble envelope, $A = (\rho_H - \rho_L)/(\rho_H + \rho_L)$ is the Atwood number, g is the gravity, and t is time. Read (1984) and Youngs (1984) show that the acceleration rate α is almost a constant, with $\alpha \approx 0.063 - 0.077$ in three-dimensional (3D) experiments. The experiments have been repeated by various authors with different apparatus, and similar values of α have been obtained; we mention the experiments of Dimonte and Schneider (1996, 2000 and Dimonte (1999)), giving $\alpha = 0.05 \pm 0.01$. The theoretically determined value, $\alpha \approx 0.05$–0.06, is obtained from a bubble merger renormalization group model. See B. Cheng, J. Glimm, and D.H. Sharp (in press), and references cited there. Computation of the center of mass of the mixing zone introduces a coupling between its two edges. Therefore, a characterization of the center of mass (nearly stationary for $A \leq 0.8$, e.g.) determines the total mixing zone size in terms of α alone (Cheng, *et al.*, 1999, 2000).

The coefficient α is thus important. It characterizes the size of the mixing zone, and thus largely determines the amount of material that is mixed. It has been reported by experimentalists as being approximately universal, in the sense that it is nearly independent of the random initial conditions of an experiment.

Researchers in several laboratories have tried to reproduce the Sharp–Wheeler theoretical scaling law with the experimental value for α through numerical simulation. Most researchers report a time-dependent, decreasing value for α, ranging from 0.015 to 0.03.

These simulations are from computational codes using numerical schemes with interfacial mass diffusion. We have compared numerical simulations using a high resolution front tracking code *FronTier* with zero interfacial mass diffusion to our own simulations using an untracked total variation diminishing (TVD)-level set code with interfacial mass diffusion similar to the others. We also introduce an analytic study of the effects of mass diffusion on buoyancy reduction

Address correspondence and reprint requests to: Xiao Lin Li, Department of Applied Mathematics and Statistics, Stony Brook University, Stony Brook, NY 11794-3600, USA. E-mail: linli@ams.sunysb.edu

and we predict the numerically observed reduction in α for untracked simulations. Our main result is that all values of α (theory, experiment, simulation) are consistent if the diffusive calculation of α is renormalized to account for mass diffusion.

We also performed simulations of the Richtmyer–Meshkov instability in spherical geometry using a two-dimensional (2D) cylindrical code.

2. DIFFUSIVE AND NONDIFFUSIVE SIMULATIONS

An earlier comparison shows that *FronTier* simulations produce values for α close to agreement with experiment while untracked TVD simulations produce low values for α (see Glimm *et al.*, 2001). These comparisons were limited in the simulation time and in the penetration depth of mixing achieved. Here we extend the comparison to a later time, comparable to most other simulations. Figure 1 shows the evolution of the fluid interface in the *FronTier* simulation. The color coding displays the height through the mixing zone, and the cut plane near the bubble surface at the top of the right frame shows the location of the 5% volume fraction contour for the light fluid. Note that there are a number of light fluid bubbles at the later time. The dynamics is multimode, not dominated by a single large space filling bubble up to this time. Such a large bubble would indicate the end of any possible self-similar flow regime, as the acceleration scaling depends upon a continued growth in the transverse scale of the mixing structures. We expand on this idea. The dynamics of continued acceleration of the mixing zone edge, as expressed in the t^2 scaling in Eq. (1), depends on a continued growth of the large scale structures (the bubbles). See, for example, Sharp (1984). Bubbles grow through a process of bubble competition and merger. Thus the t^2 scaling and the determination of α requires a simulation that is still in the multimode regime, where bubble competition and merger can occur.

The $t = 0$ interface is constructed out of Fourier modes with random amplitudes and frequencies in the range of 8 to 16 modes per computational domain width. See Glimm *et al.* (2000) for further information concerning these simulations. The $2 \times 2 \times 8$ computational domain used here allows computationally efficient late time, deep penetration simulations.

Within this computational aspect ratio, the Fourier mode numbers represent a balance between the conflicting requirements of spatial resolution, favoring low numbers of modes, and late time statistical validity, favoring large numbers of modes. Except as noted, the simulations used a $128^2 \times 512$ grid. Our simulations, thus balanced, have about $12^2 = 144$ initial bubbles and a grid resolution of about 10 cells in each dimension per initial bubble. The final time considered here has about five bubbles (see Fig. 1).

A comparison of the mixing rates for the two simulations is shown in Figure 2 (left), plotting bubble height h versus Agt^2. *FronTier* has a distinctly higher growth rate than does the interface mass diffusive TVD simulation. The value of $h(t)$ is the difference between the $t = 0$ bubble height and the time t bubble height. The latter quantity is defined in terms of a 1% volume fraction, that is, the greatest height at which the fluid is 99% heavy and 1% light according to the front tracking front or the TVD level set. This definition is somewhat unstable statistically, and a few spurious oscillations associated with the definition were removed in the plots of Figure 2.

Mass diffusion is a common feature of most untracked simulation codes. Due to the interpolation constraint, numerical schemes (finite difference, finite volume) can have only first order accuracy in their spatial derivatives near a discontinuity. For a contact discontinuity, the corresponding characteristic is linear for the wave equation of the Riemann invariant

$$\frac{\partial w}{\partial t} + u\,\frac{\partial w}{\partial x} = 0, \quad \text{where } w = \rho - \frac{P}{c^2}, \tag{2}$$

and so the truncation error will spread to the interior region. Assuming that a finite difference scheme is second order in time and first order in space at a contact discontinuity, we have the equivalent equation

$$w_t + uw_x = \frac{1}{2}\,\Delta x w_{xx}, \tag{3}$$

so that the width ΔL of the numerically diffused density profile satisfies $\Delta L \sim \sqrt{\Delta x t}$. To understand the difference between the two simulations, we compare the cross-sectional density plots in a series of horizontal slices from the bubble (upper) portion of the mixing region. Figure 3 shows the cross-sectional density plots in these simulations. Observe that there is a substantial smearing out of the density across the boundary between the two fluids in the untracked TVD simulation, whereas the *FronTier* simulation maintains a sharp boundary with a discontinuous density profile throughout the simulation. As a further difference, we note the fine-scale structure size in the *FronTier* simulation in comparison to the TVD simulation.

We compute an effective Atwood number $A(t)$ as a function of time for the TVD simulations. This is determined from the highest and lowest densities in a horizontal slice, with the resulting time- and space-dependent Atwood number averaged over heights in the upper third of the mixing zone at a fixed time to get an Atwood number dependent on time alone.

In Figure 4, we plot $A(t)$ versus t for three simulations (fine and coarse grid TVD and fine grid *FronTier*). The time dependence of $A(t)$ in the *FronTier* simulation is caused purely by (small) compressibility effects. For the mass diffusive TVD simulation, the initial density contrast, $A(t = 0) = 0.5$, is almost completely washed out; the earliest time displayed shows $A(t = 2) \approx 0.15$. As new pure (heavy

https://doi.org/10.1017/S0263034603213239 Published online by Cambridge University Press

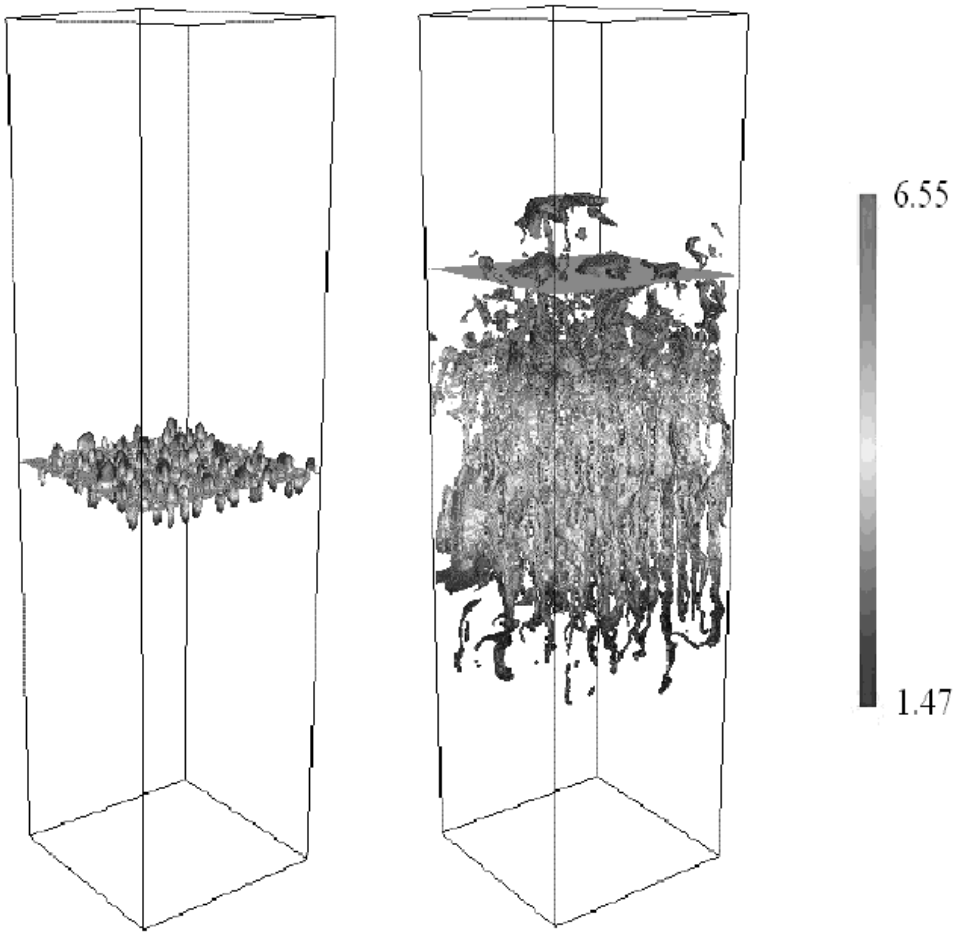

Fig. 1. Front plot for a *FronTier* simulation of Rayleigh–Taylor mixing, with $A = 0.5$. Left frame: early time. Right frame: late time. Color coding represents vertical height. The initial mean height of the interface is 4, and the height scale on the color bar applies only to the later time.

and light) fluid is injected into the mixing region, the effective Atwood number increases, but it is still reduced to about $A \approx 0.3$ on a time averaged basis, or nearly a 50% reduction relative to its initial value.

To compensate for the time-dependent Atwood number $A(t)$, we define an effective alpha, $\alpha_{eff} \approx h/2 \int\int A(s)g\, ds\, dt$ (see Fig. 2, right). Specifically, α or α_{eff} is defined here as the slope of the straight line joining the beginning and end of

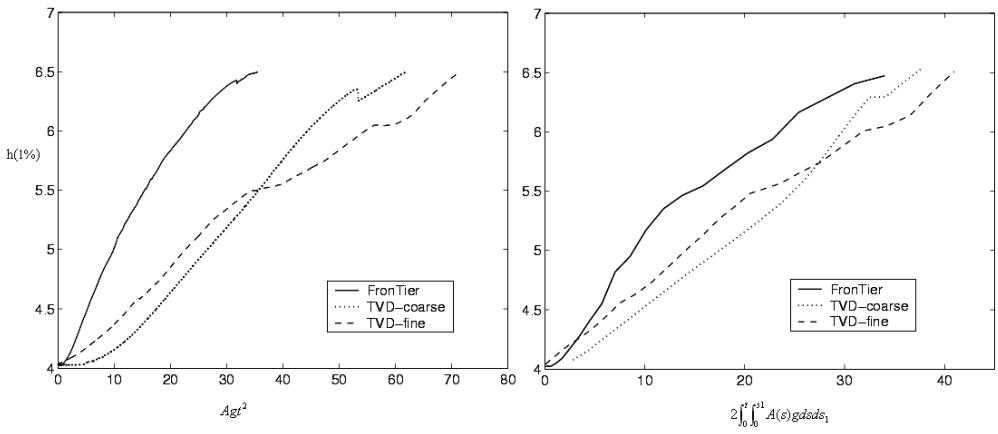

Fig. 2. Mixing growth comparison of a *FronTier* (nondiffusive) with a TVD (diffusive) simulation. For the TVD simulation, two grid levels are shown, the coarser being $64^2 \times 128$. In all cases, h is the height of the 1% volume fraction contour, and the initial mean height of the interface is 4. Left: h versus $A(t=0)gt^2$ for *FronTier* and TVD. Right: h versus $2\int_0^t\int_0^{s1} A(s)g\, ds\, ds_1$ for *FronTier* and TVD. The solid line represents the *FronTier* simulation, the dashed line is the finer grid TVD simulation, and the dotted line is the coarser grid TVD simulation.

https://doi.org/10.1017/S0263034603213239 Published online by Cambridge University Press

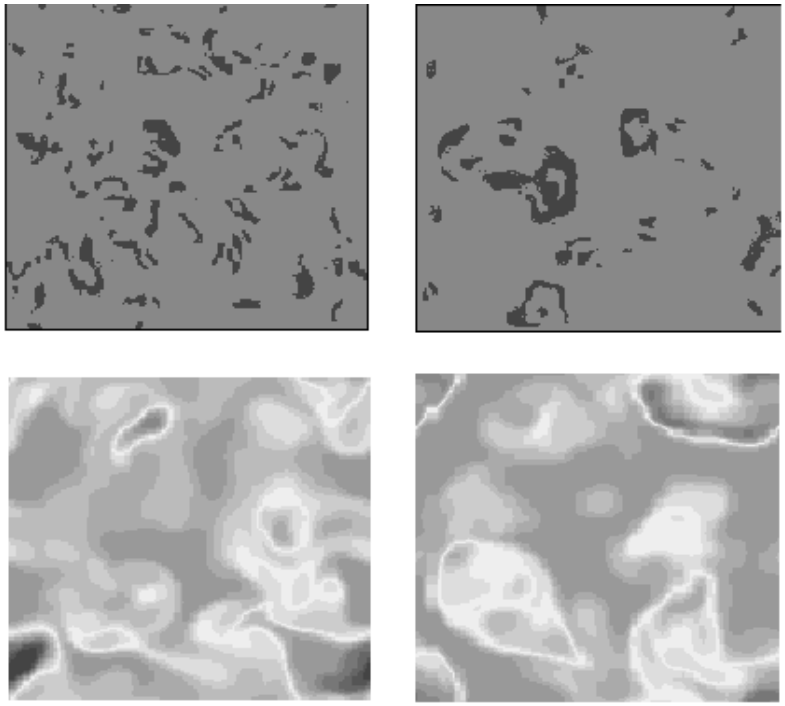

Fig. 3. Cross-sectional plots showing density on a common rainbow color scale. The pure light fluid is colored blue and the pure heavy fluid is red. Yellow and green represent various levels of microscopic mixing. The ratio of extreme density values is 3.3:1. The right frames show a higher slice in the z direction. Top: *FronTier*, bottom: TVD. The simulations are shown at comparable penetration distances, but at different times ($Agt^2 = 23$ for *FronTier*, $Agt^2 = 66$ for TVD). It is evident that the density contrast for the TVD simulation has been reduced by about 50% due to mass diffusion. See also Figure 4.

the $h(t)$ curve in Figure 2. This definition, although somewhat arbitrary, is conventional, and thus allows comparison to the results of others. We observe an improved comparison between *FronTier* and TVD and between TVD and experiment. Note that α_{eff} lies within the range of experimental values; see Table 1. On this basis, we can state that the

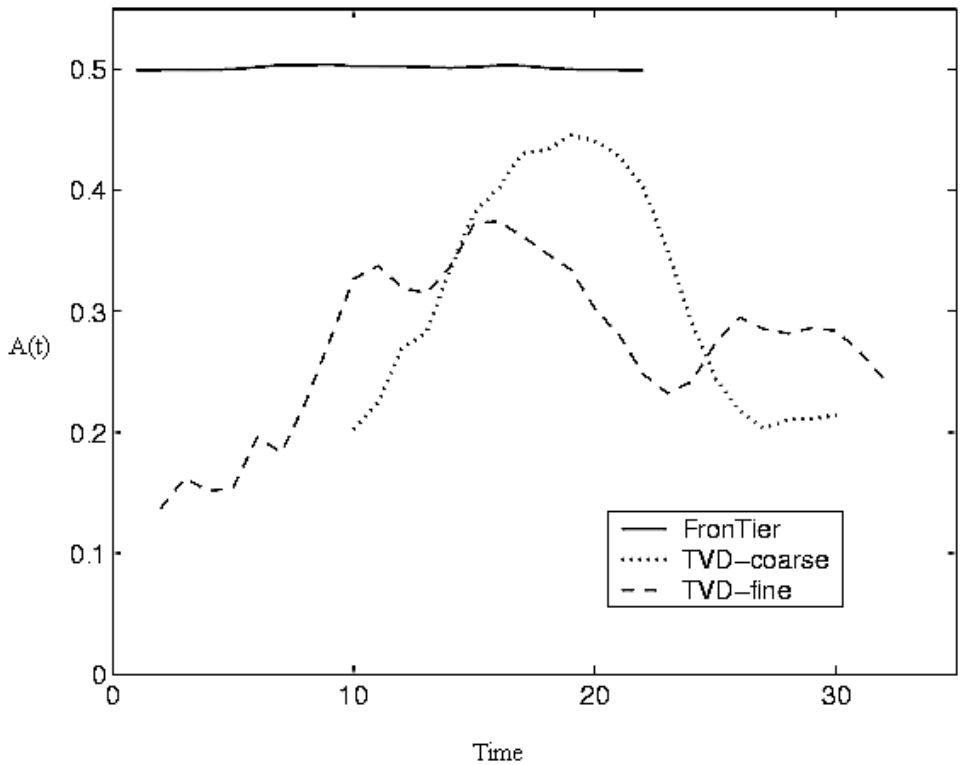

Fig. 4. Time-dependent A (Atwood number) for fine grid *FronTier*, fine grid TVD, and coarse grid $64^2 \times 128$ TVD. At time $t = 0$, all three simulations have $A(t = 0) = 0.5$. This plot displays the reduced buoyancy of the diffusive TVD simulations as a function of time.

https://doi.org/10.1017/S0263034603213239 Published online by Cambridge University Press

Table 1. *Values of α determined from experiment, theory, and simulation*

Method	α	References
Experiment	0.05–0.077	Read (1984); Youngs (1984); Dimonte and Schneider (1996, 2000); Dimonte (1999)
Theory	0.05–0.06	B.,Cheng, et al., in press
FronTier simulation (unrenormalized)	0.07	This article (Fig. 2, left); Glimm *et al.* (2001)
FronTier simulation (renormalized)	0.07	This article (Fig. 2, right)
TVD simulation (unrenormalized)	0.035	This article (Fig. 2, left)
TVD simulation (renormalized)	0.06	This article (Fig. 2, right)

All values are consistent except the unrenormalized TVD value (with α determined from a time-independent $t = 0$ Atwood number).

diffusive buoyancy renormalization of α is capable of resolving existing discrepancies among simulations, between diffusive simulations and nondiffusive experiments, and with theory.

3. DIFFUSION INDUCED BUOYANCY REDUCTION

The reduced mixing rate due to unphysical numerical diffusion can be understood from Figure 5. The left frame represents an immiscible bubble of radius r. The central and the right frame assume that this bubble is smeared out numerically to a radius R whereas the total mass inside the sphere of radius R is conserved. The buoyancy forces

$$f_1 = f_2 = \frac{4\pi r^3}{3}(\rho_h - \rho_L)g \tag{4}$$

for the bubbles in frames (a) and (c) are the same. However, due to the difference between the mass in the nondiffused bubble (a) and the diffused bubble (c), the two acceleration rates

$$a_1 = \frac{\rho_H - \rho_L}{\rho_L} g > a_2 = \frac{\rho_H - \rho_L}{\rho_L + \left(\frac{R^3}{r^3} - 1\right)\rho_H} g \tag{5}$$

are different.

As a result of the mass diffusion, the buoyancy force is distributed to a larger amount of mass, thus reducing the acceleration of the bubble.

4. RICHTMYER–MESHKOV INSTABILITY

We have performed verification and validation studies for axisymmetric simulations using *Fon Tier.* The validation was through comparison to laser driven hemispherical targets (Cheng *et al.*, 2000), and will not be repeated here. In Figure 6, we present the results of a mesh refinement study for an axisymmetrically perturbed spherical Richtmyer-Meshkov problem, comparing the growth rates as a function of time for a 200 × 200 and a 400 × 400 mesh. The influence of the symmetry axis (the "North Pole" effect on the statistical characterization of the instability evolution was studied (Glimm *et al.*, 2000; in press *a*; in press *b*), with the main conclusions that: (1) the effect was a real consequence of axisymmetrically perturbed flows, i.e., it was not due to

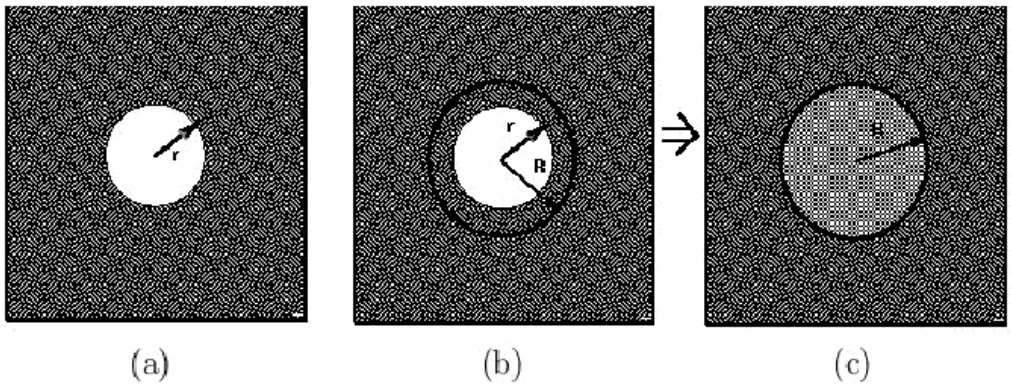

Fig. 5. Left: Unmixed bubble of light fluid. Center: Unmixed bubble and heavy fluid mass that will be mixed with it. Right: Mixed bubble.

https://doi.org/10.1017/S0263034603213239 Published online by Cambridge University Press

numerical effects, (2) it was independent of spherical flow geometry, and arises in cylindrically shaped flows, (3) that the effect occurs late in time and for spherical flows, is pronounced after reshock, and (4) that the effect is not eliminated through use of spherical harmonic (Legendre polynomial) perturbations.

We present in Figure 7 the results of a strong shock scaling law analysis of the mixing zone growth rate for a spherically perturbed Richtmyer-Meshkov problem. The perturbed spherical surface separates a heavy gas (on the interior) from a light gas (on the exterior), with the initial shock location in the heavy fluid, facing outward (explosion). Following Zhang and Graham (1997), where a similar scaling law was introduced for cylindrical implosions, we scale the velocity and times by the incident shock Mach number, introducing a scaled velocity $v' = v/M$ and time $t' = Mt$. The results of the scaling show a near identity of growth rate curves, which is remarkable in view of the large amount of structure in the curves themselves. Again the configuration is heavy exploding light.

5. CONCLUSION

We present a *FronTier* simulation run to late time and deep penetration. The simulation is terminated while still in a multimode regime. It has no interfacial mass diffusion, and the overall bubble mixing rate lies within the experimental range. We recalibrate the buoyancy force for mass diffusive TVD simulations, and obtain a renormalized α_{eff} that is also in agreement with experiment. On this basis, the nondiffusive simulation and the theory of mass diffused buoyancy reduction presented here are capable of resolving the principal differences between simulation and experiment for Rayleigh–Taylor mixing. Our results confirm the earlier agreement between theory and experiment (see B. Cheng, J. Glimm, and D. H. Sharp, in press). Finally, we observe that our results open a door to further research, and do not close inquiry related to the determination of the mixing rate, as the uncertainties in the experimental, theoretical, and simulation determination of α deserve further investigation. Concerning simulation, which is the main thrust of this article, we mention the importance of improved resolution. The needs for resolution are numerical accuracy, governed by mesh cells per bubble, statistical accuracy, governed by the number of bubbles, especially at the end of the simulation, and convergence to self-similar flow, governed by the length of time of the simulation.

REFERENCES

Cheng, J., Glimm, J., Saltz, D. & Sharp, D.H. (1999). Boundary conditions for a two pressure two phase flow model. *Physica D* **133**, 84–105.

Cheng, B., Glimm, J. & Sharp, D.H. (2000). Density dependence of Rayleigh–Taylor and Richtmyer–Meshkov mixing fronts. *Phys. Lett. A* **268**, 366–374.

Cheng, B., Glimm, J. & Sharp, D.H. (in press). A 3D RNG bubble merger model for Rayleigh–Taylor mixing. *Chaos.*

Dimonte, G. (1999). Nonlinear evolution of the Rayleigh–Taylor and Richtmyer–Meshkov instabilities. *Phys. Plasmas* **5**, 2009–2015.

Dimonte, G. & Schneider M. (1996). Turbulent Rayleigh–Taylor instability experiments with variable acceleration. *Phys. Rev. E* **54**, 3740–3743.

Dimonte, G. & Schneider M. (2000). Density ration dependence of Rayleigh–Taylor mixing for sustained and impulsive acceleration histories. *Phys. Fluids* **12**, 304–321.

Drake, R.P., Robey, H.F., Hurricane, O.A., Remington, B.A., Knauer, J., Glimm, J., Zhang, Y., Arnett, D., Ryutov, D.D., Kane, J.O., Budil, K.S. & Grove, J.W. (2002). Experiments to produce a hydrodynamically unstable spherically diverging system of relevance to instabilities in supernovae. *Astrophy. J.* **564**, 896–906.

Glimm, J., Grove, J.W., Li, X.L., Oh, W. & Sharp, D.H. (2001). A critical analysis of Rayleigh–Taylor growth rates. *J. Comp. Phys.* **169**, 652–677.

Glimm, J., Grove, J.W. & Zhang, Y. (2000). Three dimensional axisymmetric simulations of fluid instabilities in curved geometry. In *Advances in Fluid Mechanics III* (Rahman, M. & Brebbia, C.A., Eds.). pp. 643–652. Southampton, UK: WIT Press.

Glimm, J., Grove, J.W. & Zhang, Y. (in press *a*). Interface tracking for axisymmetric flows. *SIAM J. Sci. Comp.*

Glimm, J., Grove, J.W., Zhang, Y. & Dutta, S. (in press *b*). Numerical study of axisymmetric Richtmyer–Meshkov instability and azimuthal effect on spherical mixing. *J. Stat. Physics.*

Read, K.I. (1984). Experimental investigation of turbulent mixing by Rayleigh–Taylor instability. *Physica D* **12**, 45–58.

Sharp, D.H. (1984). *Physica D* **12**, 3–18.

Sharp, D.H. & Wheeler, J.A. (1961). Late stage of Rayleigh–Taylor instability. Technical report, Institute of Defense Analyses.

Youngs, D.L. (1984). Numerical simulation of turbulent mixing by Rayleigh–Taylor instability. *Physica D* **12**, 32–44.

Zhang, Q. & Graham, M.J. (1997). Scaling laws for unstable interfaces driven by strong shocks in cylindrical geometry. *Phys. Rev. Lett.* **79**, 2674–2677.

https://doi.org/10.1017/S0263034603213239 Published online by Cambridge University Press